Electronics and Electrical Engineering

http://www.aimspress.com/journal/ElectrEng

AIMS Electronics and Electrical Engineering, 6(3): 296–316.
DOI: 10.3934/electreng.2022018
Received: 17 June 2022
Revised: 13 August 2022
Accepted: 22 August 2022
Published: 26 August 2022

Research article

Improved DTC strategy with fuzzy logic controller for induction motor driven electric vehicle

Anjan Ku. Sahoo[1,*], **and Ranjan Ku. Jena**[2]

[1] Department of Electrical Engineering, BPUT, Rourkela, Odisha, INDIA
[2] Department of Electrical Engineering, CAPGS, BPUT, Rourkela, Odisha, INDIA

* **Correspondence:** Email: anjank.sahoo@gmail.com.

Abstract: In the near future, zero-emission transportation is anticipated to be implemented in an effort to reduce the major pollutants caused by road transportation. This enormous endeavor will be impossible until all modes of transport are electrified. The induction motor-fed direct torque controller is widely used for EV applications due to its fast torque response and simplicity. However, ripples in torque and flux and current harmonics are the major issues related to DTC. The fuzzy-based DTC replaces the hysteresis comparators and the switching table with fuzzy logic blocks to realize fuzzy DTC control, which improves the system's performance. This paper presents an enhanced fuzzy logic control strategy of induction motor for electric vehicle applications. The main objective is to enhance the system's performance by reducing torque and flux ripples. Both the conventional and fuzzy-based DTC are simulated with MATLAB/SIMULINK, followed by a comparative assessment to validate the effectiveness of the proposed approach for both steady-state and transient operations. The results indicate improvements in torque ripple, flux ripple, and speed ripples by 69%, 10%, and 85%, respectively. Due to the reduction in ripples, there is also an improvement in the THD of the stator current by 17%. During transient, an average improvement of integral square error for torque and speed is 8% and 12%, respectively. Further, the proposed method is validated using EUDC and HWFET drive cycles, demonstrating a reduction in battery energy demand.

Keywords: electric vehicle; torque ripple; direct torque control; fuzzy logic; induction motor

1. Introduction

The electric car revolution has intensified over the past two decades due to increased environmental concerns and a desire to reduce reliance on conventional fuels for transportation. Even though gasoline-powered vehicles are the most frequent type of vehicle; their tailpipe emissions create air pollution and contribute to greenhouse gas emissions. The United Nations presented all nations with

goals and timelines concerning the reduction of carbon emissions [1]. Transportation is the major contributor to greenhouse gas emissions, including carbon dioxide, methane, and other toxins [2]. Road transportation accounts for roughly half of urban greenhouse gas emissions. The transportation industry is responsible for approximately 14% of the world's annual greenhouse gas emissions, with 72 percent of those emissions come from automobiles [2, 3]. The industrial expansion's emphasis on transportation causes a long-term environmental hazard. The road transportation sector's impacts on the atmosphere and the worldwide depletion of fossil fuels must be mitigated by the implementation of measures [3]. Considering and developing electric vehicles (EVs) due to their climate-friendly characteristics is one of the most important answers to the present environmental problems. Zero emissions, ease of use, and dependability [1, 4, 5]. Due to this rapid transition, the electric vehicle (EV) sector faces unique problems and calls for unique tactics. EVs are primarily un-affordable due to their limited range and high price [4, 5].

For the urban driving scenario, the asynchronous motor is the most suitable for traction application because of its durability, low cost, lower maintenance requirements, and higher efficiency [6]. Direct torque control (DTC) and indirect field-oriented control (IFOC) are used for IM to provide a quick transient response from the motor drives. Due to its simple structure, rapid dynamic response, robustness to rotor parameters, and greatly simplified inverter control structure, the DTC is extensively employed and one of the most suitable choices for electric vehicle applications. It provides a faster torque response with separate control of the flux and torque. However, using hysteresis controllers results in significant torque and flux ripples, a considerably high starting current, variable switching frequency, and sluggish response during low-speed regions [7]. The negligence of stator resistance influences performance at a low speed [8]. The torque ripples result in undesirable acoustic noise and mechanical vibration, degrade the performance and increase current harmonics leading to poor output power quality. Furthermore, the practical implementation of hysteresis-type nonlinear elements demands a low sampling period and, thus, a high calculation frequency, resulting in architectural constraints. Nonetheless, DTC exhibits promising outcomes in several circumstances, especially in the field of electric vehicle application, and still, an interest in research for further improvement.

Despite its simplicity, robustness, fast response, ripples in flux and torque, current distortion, and high switching losses are the main challenges of DTC [9]. Thus DTC has undergone numerous studies to improve its performance, specifically to reduce the ripples and improve efficiency. In [8], several classical and advanced DTC schemes are reviewed, including algorithm complexity, switching loss, and parameter sensitivity. AI-based strategies such as ANN, FLC, and GA are compatible with DTC for ripple mitigation, THD reduction, efficiency enhancement, and energy savings of IM with a cost of system complexity and higher computational time. This achievement is attributable to the fact that artificial intelligence can easily approximate the control behavior of human experts who often operate in poor contexts. ANN combined with DTC was proposed by [10]. However, this requires parallel processing due to its high complexity. The network structure is achieved through trials as there is no specific process for defining the algorithm. As a result, the practical realization is limited. SMC is one of the robust and non-linear mechanisms to improve DTC. The SMC-based DTC method described in [11] efficiently drives an electric vehicle employed with a four-wheel motor drive. This has the advantage of parameter insensitivity and better dynamic response, whereas it suffers from the "chattering" phenomenon causing high harmonics. In [12] SPWM based DTC with constant switching frequency is presented, which offers low THD, switching losses, and ripples; however, it does not

provide satisfactory performance with external disturbances and parameter variation due to the use of a PI controller.

Recently, FLC has been spotlighted as one of the most promising DTC application techniques. FLC has been applied to industrial automation and vehicle propulsion systems in various ways, and much research has been going on for further improvement. FLC for induction motor drives has been studied for speed and torque control, ripple minimization, THD reduction, efficiency optimization, and energy management [13]. The operation of FDTC is identical to that of standard DTC, except for absence of flux, torque, and hysteresis bands. Due to its stable performance and reduced mathematical dependence on actual plant data, the FLC has many advantageous characteristics. *Gdaime et al.* [14] examine the conceptual and practical use of a fuzzy logic controller integrated with a DTC drive to regulate an IM. A fuzzy logic controller replaces the lookup table and hysteresis controllers. It takes flux error, torque error, and stator flux angle as input variables and provides the inverter switching state as output. An FLC-based DTC was proposed in [15] for reducing torque and flux ripples in IM while improving stator current waveforms with a parallel sliding mode speed controller and stator flux MRAS observer. However, dynamic behaviour reduces the ripples, with a cost of higher system complexity. Fuzzy Duty Cycle Controller and Fuzzy Logic Switching Controller are integrated with DTC to reduce flux and torque ripple of IM drive in [16]. The results indicate a steady stator flux trajectory with improved transient performance. The fuzzy logic control integrated with the DTC that drives an IM through a standard two-level inverter is provided in [17] with an estimator that transitions from SMO at low speed to a combined SMO and MRAS estimator at high speed. In [18], a novel switching table is proposed using FLC to control the switching frequency of a doubly fed IM powered by two VSI. The proposed approach reduces torque ripple and improves the current shape by optimizing the THD. A Fuzzy-PI-controlled quasi-ZSI IM drive is presented in [19]. The Fuzzy-PI controller is used as a speed regulator to eliminate the torque ripple and SMC chattering of the IM with an improvement in convergence rate.

Finally, all of these algorithms have their advantages and disadvantages. So the choice of the control algorithm for induction motor in propulsion depends on cost, accuracy, and durability. A fuzzy logic controller is most suitable where the system behavior is more complicated and semantic rules are necessary to explain the system. Among the AI techniques, Fuzzy logic controllers are effective at dealing with the uncertainty of the DTC switching table [20], particularly during transient phenomena. As discussed in [8], it provides a fast dynamic torque response with significantly lower ripples and THD than other conventional and AI-based DTC. As it is insensitive to parameter variation provides a good dynamic response at low speed with a low switching loss. The FLC can handle both sophisticated and poorly modeled systems. In addition, it offers reliable performance and little mathematical reliance on system parameters [21]. Due to these reasons, an FLC-based DTC is considered for the IM-driven EV in this work to reduce torque ripples and improve performance. The drive is modelled using the FIS toolbox in MATLAB/SIMULINK to assess and compare it to the standard DTC. The torque, flux ripples, and stator current harmonics are evaluated under distinct torque profiles and load circumstances. The performance during transient is evaluated considering ISE as a parameter. The results indicate a significant reduction in the ripple with improved performance. Finally, both conventional and fuzzy DTCs are compared to standard drive cycles.

This paper presents a comparative study between the classical DTC and Fuzzy based DTC controller, organized as follows: after the introduction in the first section in section 2, the vehicle's modelling is given. In section 3, explanations of the traditional DTC are provided, while section 4

explains the suggested Fuzzy DTC. Section 4 presents simulation findings and discussions, whereas Section 5 concludes the work.

2. Vehicle dynamics

The driving power and energy required to assure vehicle operation can be calculated using vehicle mechanics and aerodynamics concepts, as shown in Figure 1 [22].
The power P_v is necessary to drive the vehicle at speed 'v' and compensates for the load.

$$P_v = vF_{te} = v\left(F_{ro} + F_{cr} + F_{ad} + F_{la}\right) \tag{2.1}$$

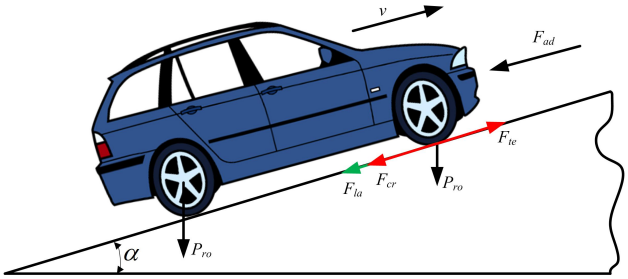

Figure 1. Elementary force acting on the vehicle.

The propulsion system's motive power F_{te} partially overcomes the road load. The vehicle is accelerated by the net force $(F_{te} - F)$ (or decelerates when F exceeds F_{te}). As a result, the acceleration is given by:

$$a = \frac{dv}{dt} = \frac{F_{te} - F}{k_m m} \tag{2.2}$$

The mechanical equations describing each wheel drive are as follows:

$$J\frac{d\omega_m}{dt} + T_B + T_L = T_{em} \tag{2.3}$$

Due to the employment of a reduction gear, the wheel velocity and torque are represented by.

$$\begin{cases} \omega_{wheel} = \frac{\omega_m}{i} \\ T_{wheel} = T_m i \eta_i \end{cases} \tag{2.4}$$

The mechanical torque of the motor is described by:

$$T_m = \frac{T_{\text{wheel}}}{i} = \frac{R}{i}F_\omega \tag{2.5}$$

The global moment of inertia of the vehicle in the motor referential is provided by:

$$\begin{cases} J = J_W + J_v \\ J_v = \frac{1}{2}m\frac{R^2}{i^2}(1 - \lambda) \end{cases} \tag{2.6}$$

If the road surface has a high adhesion coefficient, then λ is usually negligible and can be ignored.

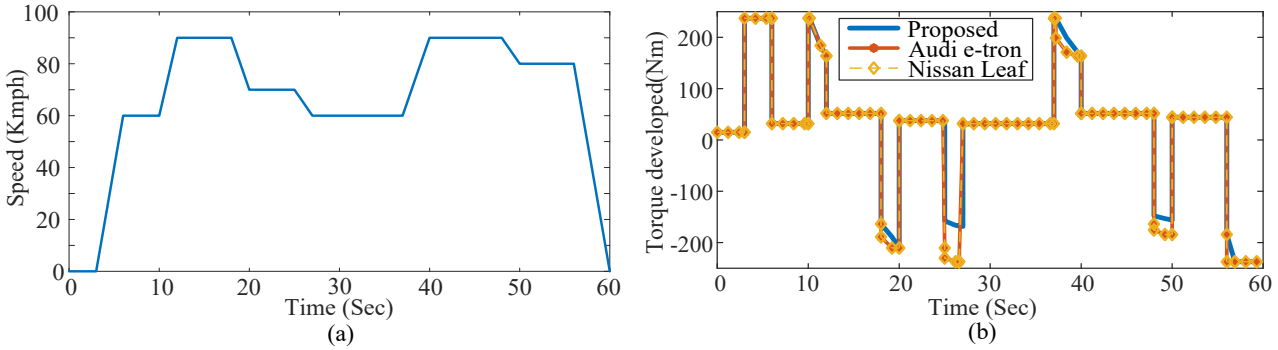

Figure 2. Vehicle dynamics (a) applied speed (d) corresponding torque developed.

The curb and gross weight of some popular electrical vehicles are listed in Table 1. The gross weight of the vehicle is composed of its curb weight and payload. A similar weighted vehicle is considered for investigation in this work. The parameters and other specifications of the vehicle under consideration in this work are presented in Table 2. These are based on the currently available 5-seaters available in the market.

Figure 2(a) depicts a realistic driving scenario for the purpose of analyzing the vehicle's dynamic performance. The torque profile of Figure 2(b) indicates a small torque requirement at a constant speed, however; during acceleration, there is a significant increase in torque required to meet the load demand. Negative torque demand during braking ensures regenerative braking and rapid speed changes.

Table 1. Curb and gross weights of some popular EVs.

Make & Model	Curb weight (in Kg)	Grog weight (in Kg)
Audi e-tron	2560	3200
BMW i3	1501	1951
Chevrolet Bolt	1616	2113
Fiat 500e	1361	1811
Ford Mustang Mach-E	2100	2600
Hyundai Kona	1743	2243
Kia Niro	1748	2298
MG ZS	1539	2039
Nissan Leaf	1680	2180
Porsche Taycan	2305	2805
Renault Kangoo	1410	2126
Renault Zoe	1470	1965
Tesla X P100D	2509	3109
Volkswagen e-Golf	1615	2115

Table 2. Parameters of the vehicle under consideration in this work.

Parameter	Value	Parameter	Value	Parameter	Value
Curb weight	1245 kg	Rolling resistance coefficient	0.015	Maximum speed	130 Kmph
Gross weight	1645 Kg	Frontal area	2.3 m^2	0 – 60 kmph acceleration time (tm)	≤ 15 sec
Wheel Radius (r)	0.315 m	Aerodynamics drag coefficient	0.275	Air density	1.25 kg/m^3

The torque required to propel the vehicle at a specific driving scenario is the reference load torque of the induction motor. Figure 2(b) indicates the required torque for the proposed vehicle used in this work and for the Audi e-tron and Nissan Leaf. As seen from the results, a similar torque profile is required by all the vehicles, and as presented in [23], the same model is also applicable with a variation in wheel diameter, torque speed profile, and other variations of vehicle parameters.

3. Conventional direct torque control

In the middle of the 1980s, Takahashi [24] and Depenbrock [25] came up with the concept of the direct torque control for controlling the speed and torque of an induction motor. It is mostly independent of variation in machine parameters, and its control technique is more straightforward as a result of the absence of current controllers and pulse width modulations. The use of DTC control ensures that the operation will be very efficient and provides minimal speed error and quick torque response.

The accuracy of the torque and flux estimation is absolutely necessary for achieving the best possible performance in DTC. Therefore, it is necessary to establish numerous factors based on the stator current and stator voltage. These parameters are converted to (d, q) coordinates using the DTC-optimized Concordia transformation.

The induction motor equation in state variable form can be expressed as:

$$\frac{d}{dt}\begin{bmatrix} \overline{\psi}_s \\ \overline{\psi}_r \end{bmatrix} = \begin{bmatrix} \frac{-R_s}{\sigma L_s} & \frac{R_s L_m}{\sigma L_s L_r} \\ \frac{R_r L_m}{\sigma L_s L_r} & j\omega - \frac{R_r}{\sigma L_s L_r} \end{bmatrix} \begin{bmatrix} \overline{\psi}_s \\ \overline{\psi}_r \end{bmatrix} + \begin{bmatrix} 1 \\ 0 \end{bmatrix} \overline{v}_s \tag{3.1}$$

Based on equation 3.1 The stator flux in (d, q) coordinates can be estimated as shown in equation 3.2

$$\begin{cases} \psi_{ds}(t) = \int \left(V_{ds}(t) - R_s i_{ds}(t)\right) dt \\ \psi_{qs}(t) = \int \left(V_{qs}(t) - R_s i_{qs}(t)\right) dt \end{cases} \tag{3.2}$$

The stator flux and motor torque can be estimated using equation 3.2 as follows:

$$\psi_s = \sqrt{\psi_{ds}^2 + \psi_{qs}^2} \qquad and \qquad \theta_s = \tan^{-1} \frac{\psi_{qs}}{\psi_{ds}} \tag{3.3}$$

$$T_e = \frac{3pL_s}{2\sigma L_s L_r} \psi_s \cdot \psi_r \cdot \sin\gamma \tag{3.4}$$

With appropriate stator voltage control, the electromagnetic torque can be controlled by varying γ.

For simplicity neglecting stator resistance as it is small the stator flux over one sampling interval can be expressed as:

$$\Delta\psi_s = V_s \Delta t \tag{3.5}$$

As per Equation 3.2, the stator flux can be regulated by applying a suitable voltage vector over one sampling period. The estimated electromagnetic torque T_{est} and flux ϕ_{est} values are compared to their corresponding reference values T^*_{em} and ϕ^*_s by using the three-level and two-level comparators respectively. These error signals are used as input to the optimal switching table for selecting appropriate stator flux increments and establishing the flux within the prescribed hysteresis band, as seen in Figure 3. The response of the comparators is represented as ΔT_e and $\Delta\Psi_s$, respectively, as indicated in Equations 3.6 and 3.7, where HBT_e and $HB\Psi$ denote the hysteresis controller's bandwidths for electromagnetic torque and stator flux, respectively. Table 3 provides an outline of the output voltage vector for each sector.

Table 3. Switching table for classical DTC.

$\Delta\phi$	ΔT_e	S_1	S_2	S_3	S_4	S_5	S_6
1	1	V_2	V_3	V_4	V_5	V_6	V_1
	0	V_7	V_0	V_7	V_0	V_7	V_0
	-1	V_6	V_1	V_2	V_3	V_4	V_5
0	1	V_3	V_4	V_5	V_6	V_1	V_2
	0	V_0	V_7	V_0	V_7	V_0	V_7
	-1	V_5	V_6	V_1	V_2	V_3	V_4

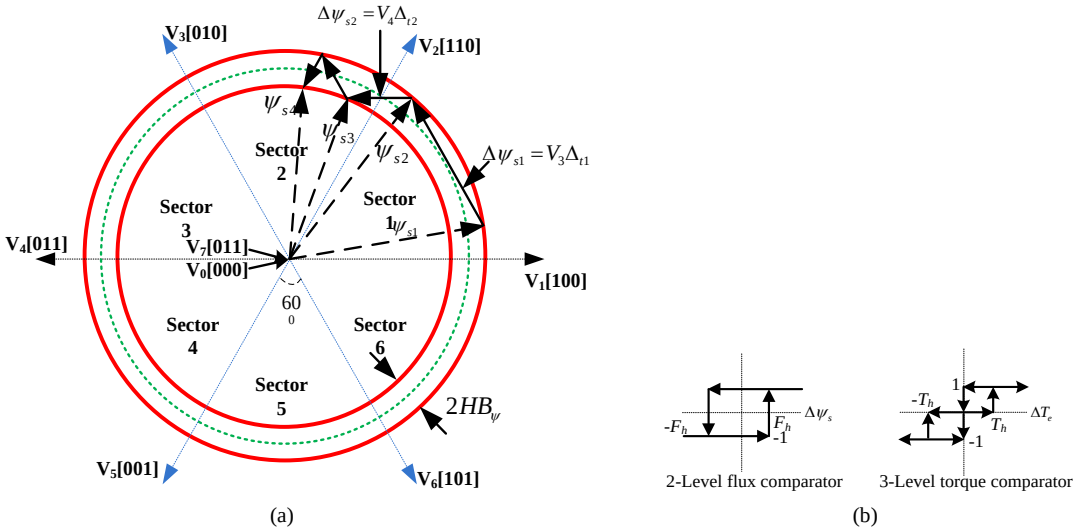

Figure 3. Classical DTC.

$$HT_e = \begin{cases} 1 & for\ \Delta T_e > HBT_e \\ 0 & for\ -HBT_e < \Delta T_e < HBT_e \\ -1 & for\ \Delta T_e < -HBT_e \end{cases} \tag{3.6}$$

$$H_\psi = \begin{cases} 1 & for\ \Delta\psi_s > HB_\psi \\ -1 & for\ \Delta\psi_s < -HB_\psi \end{cases} \tag{3.7}$$

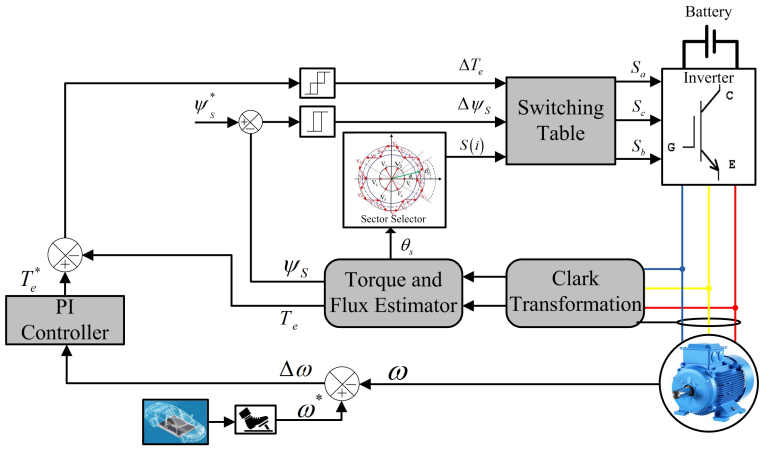

Figure 4. Classical DTC.

Figure 4 presents the block diagram depicting the principal DTC approach applied to an electric vehicle. Voltage source inverter, motor, torque and flux estimator, hysteresis regulator, and switching table are the components that make up the design structure.

The DTC control is not without serious flaws, in spite of the fact that it is simple to operate, long-lasting, and quick. The employment of torque and flux hysteresis controllers results in significant flux and torque ripples, which cause structural vibrations, unenviable acoustical noise, and consequently a decrease in overall performance. Additionally, classical DTC also results in variable switching frequency and current harmonics, both of which tends to deteriorate the output power quality. Neglecting to pay attention to the stator resistance might lead to problems at low speeds. Additionally, the successful integration of hysteresis-type nonlinear elements calls for a sampling time that is relatively short, and as a result, a high computation frequency places limitations on the architectures that may be used.

4. Fuzzy direct torque control

Similar to classic DTC, fuzzy logic direct torque control (FDTC) operates on the same basic concept. Keeping the basic structure, the same in FDTC the hysteresis comparator and the switching table are replaced by a fuzzy logic controller, and the PI speed controller can be replaced by a fuzzy logic speed controller. FLC combined with DTC provides a reduction in torque and flux ripples without knowledge of the mathematical model of the plant and the capability of handling non-linearity [20]. Figure 5 depicts the fuzzy DTC with an induction motor proposed for EV application.

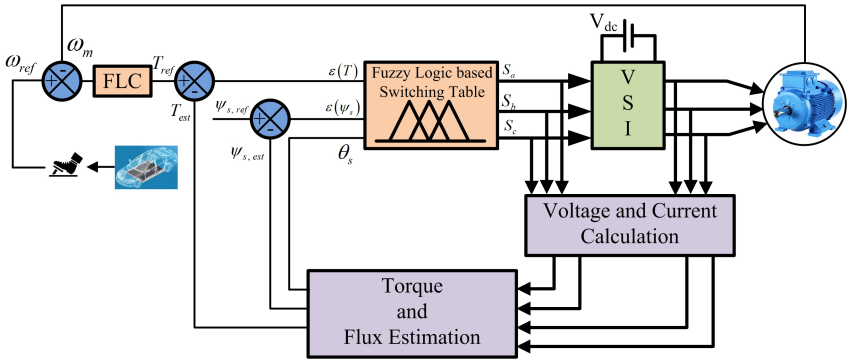

Figure 5. Fuzzy DTC.

In conventional DTC, the large magnitude of ripples results from constant magnitude hysteresis bands utilized to determine the inverter switching state without considering the extent of the error. Hence, the switching state selected for a large error appearing during a transient is the same as when the error is small during steady operation; consequently, the response is systematically imprecise. If the voltage vector is selected based on the magnitude of torque and flux errors, system performance can be enhanced. In order to accomplish this, a concept of large and small errors is included in the fuzzy system, which employs distinct voltage vectors for each.

The flux error($\varepsilon(\psi_s) = \psi_{s,ref} - \psi_{s,est}$), torque error($\varepsilon(T) = T_{ref} - T_{est}$), and the position of the stator flux vector are inputs to the fuzzy switching table [22]. The output of the fuzzy switching table is connected to the switches of the VSI. Each input and output is divided into a pre-set number of fuzzy sets to increase control and reduce ripple with the fewest rules possible. As a mathematical model, fuzzy logic is based on the membership and Degree of Membership principles, which contain several logic values and truth values ranging from 0 to 1. To specify the torque error for DTC drives, a specific range is divided into membership functions that govern the high ripple factor. The steps utilized for FLC are:

1. **Fuzzification**: In this process, the analog inputs are turned into fuzzy membership variables. Here the analog inputs are the flux error, torque error, and stator flux angle. Figure 6 displays the membership functions used by the fuzzy logic algorithm in this work.

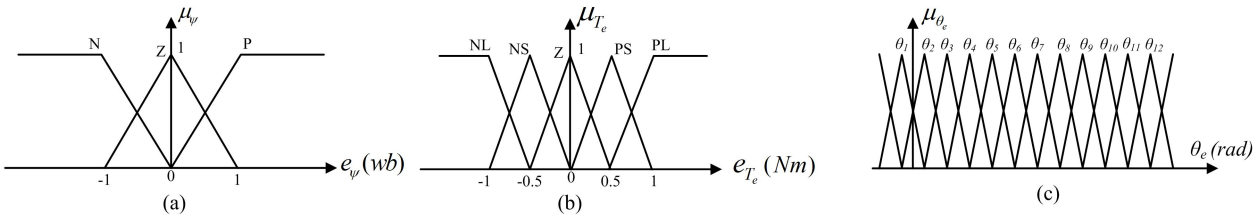

Figure 6. Fuzzy input membership functions.

To achieve optimal stator flux variations, three overlapping fuzzy sets, including negative (N), zero (Z), and positive (P), are introduced, and normalized to [-1, 1]. The fuzzy variables N and P are represented by trapezoidal membership functions, whereas variable Z is represented by a

triangular membership function for simplicity and ease in implementation as shown in Figure 7(a) [20]. For flux error, $\varepsilon(\psi_s) \geqslant 0.04wb$ is regarded as 'P' and $\varepsilon(\psi_s) \leqslant -0.04wb$ is regarded as 'N' with membership values 1 and -1 respectively. For error within these values, the membership reduces linearly to reach 0 when $\varepsilon(\psi_s) = 0$.

However, the torque error MF included five overlapping fuzzy sets, including negative large (NL), negative small (NS), zero (Z), positive small (PS), and positive large (PL), in an effort to permit smaller torque variations. The NL and PL are constituted by trapezoidal membership functions and NS, Z, and PS are constituted by triangular membership functions as shown in Figure 7(b). For flux error, $\varepsilon(T) \geqslant 20N.m.$ is regarded as 'PL' and $\varepsilon(T) \leqslant -20N.m.$ is regarded as 'NL' with membership values 1 and -1 respectively, with the reduction in torque error membership value reduces linearly and reaches 0 when $\varepsilon(T) = 10N.m.$ and the membership value for 'PS' becomes 1, hence the error is considered as positive small. Similarly, with a further decrement in membership value, PS reduces linearly and becomes 0 when $\varepsilon(T) = 0$, and the membership value of 'Z' will be 0. Accordingly, the membership values of 'NS' can be estimated. The membership value in the overlap region is determined using the min-max method.

In addition, the stator flux orientation is divided into 12 sectors, allowing for more precision in the fuzzy variable selection, which is consistently represented by 60^0-wide triangular membership functions overlapping 30^0 with adjacent fuzzy sets. So that each fuzzy set functions for a 30^0 angle, as illustrated in Figure 7(c) [14]. The range of the stator flux angle is [0, 2π].

Figure 11 depicts the fuzzy controller output variable, which consists of eight singleton subsets $(V_0 - V_7)$. Out of which two are zero-voltage vectors ($V_0 and V_7$), while the remaining six $(V_1 - V_6)$ are nonzero voltage vectors.

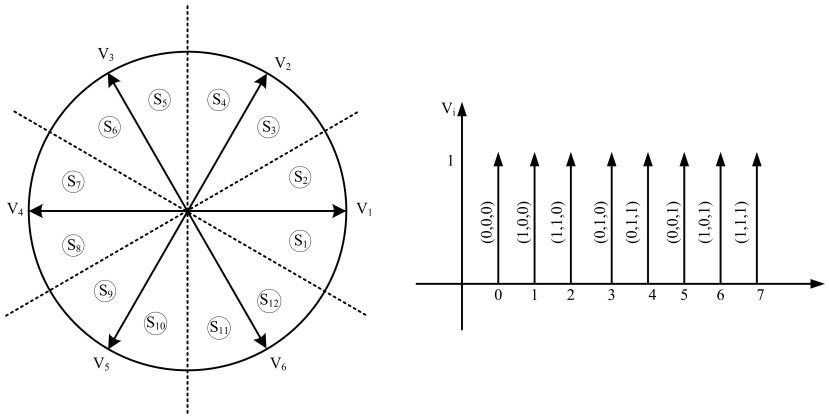

Figure 7. Fuzzy output membership functions.

2. **The fuzzy interference engine**: By linking the input and output variables with the fuzzy rules, the fuzzy interference engine performs approximation reasoning. The inference rules are constructed so that disparities between the flux and torque set points and their estimated values can be adjusted. Here, Mamdani's max-min choice approach is employed, due to its low complexity in implementation and better results. Assuming μ_A, μ_B, μ_C, and μ_V as the membership functions, the weight factor 'α_i' for the i^{th} rule can be estimated as

$$\alpha_i = min(\mu_{Ai}(e_\psi), \mu_{Bi}(e_T), \mu_{Ci}(\theta)) \tag{4.1}$$

The output membership function is then given by:

$$\mu'_{Vi}(v) = max(\alpha_i, \mu_{Vi}(V)), i = 1, 2, 3, ...180 \tag{4.2}$$

3. **Fuzzy rule base**: It characterizes the operation of a fuzzy system. The fuzzy rules described are expected to facilitate control that maintains the stator flux at the reference value while enabling a rapid torque response [14]. The three input variables and the output variable can define the control rules; hence, equation 4.3 [14] can be used to generalize the i_{th} rule.

$$R_i : If\ e_\psi\ is\ A_i\ \&\ e_T\ is\ B_i\ \&\ \theta_e\ is\ C_i,\ then\ 'v'\ is\ V_i \tag{4.3}$$

Where, $A_i, B_i, and C_i$ indicate fuzzy sets for the variables $e_\psi, e_T, and \theta_e$respectively. Additionally, V_i is the fuzzy output for rule i.
The purpose of the control system is to maintain the stator flux at a predetermined operating state with a rapid torque response. The rule base is derived from the diagram illustrated in Figure 7. For example, if the stator flux orientation is located in the sector 2 interval, when one wishes to decrease the torque and increase the flux then the V_1 vector is the best choice. The identical principle is used to build the 180 rules base for the fuzzy controller presented in Table 4.

Table 4. Fuzzy controller table for voltage vectors.

e_ψ	e_{T_e}	θ_1	θ_2	θ_3	θ_4	θ_5	θ_6	θ_7	θ_8	θ_9	θ_{10}	θ_{11}	θ_{12}
P	PL	V_2	V_3	V_3	V_4	V_4	V_5	V_5	V_6	V_6	V_1	V_1	V_2
	PS	V_2	V_2	V_3	V_3	V_4	V_4	V_5	V_5	V_6	V_6	V_1	V_1
	Z	V_0	V_7	V_7	V_0	V_0	V_7	V_7	V_0	V_0	V_7	V_7	V_0
	NS	V_1	V_1	V_2	V_2	V_3	V_3	V_4	V_4	V_5	V_5	V_6	V_6
	NL	V_6	V_1	V_1	V_2	V_2	V_3	V_3	V_4	V_4	V_5	V_5	V_6
Z	PL	V_2	V_3	V_3	V_4	V_4	V_5	V_5	V_6	V_6	V_1	V_1	V_2
	PS	V_2	V_3	V_3	V_4	V_4	V_5	V_5	V_6	V_6	V_1	V_1	V_2
	Z	V_7	V_0	V_0	V_7	V_7	V_0	V_0	V_7	V_7	V_0	V_0	V_7
	NS	V_7	V_0	V_0	V_7	V_7	V_0	V_0	V_7	V_7	V_0	V_0	V_7
	NL	V_6	V_1	V_1	V_2	V_2	V_3	V_3	V_4	V_4	V_5	V_5	V_6
N	PL	V_3	V_4	V_4	V_5	V_5	V_6	V_6	V_1	V_1	V_2	V_2	V_3
	PS	V_4	V_4	V_5	V_5	V_6	V_6	V_1	V_1	V_2	V_2	V_3	V_3
	Z	V_7	V_7	V_0	V_0	V_7	V_7	V_0	V_0	V_7	V_7	V_0	V_0
	NS	V_5	V_5	V_6	V_6	V_1	V_1	V_2	V_2	V_3	V_3	V_4	V_4
	NL	V_5	V_6	V_6	V_1	V_1	V_2	V_2	V_3	V_3	V_4	V_4	V_5

4. **De-fuzzification**: This process aims to convert the fuzzy output into an analogue value that may be used as an input by the controlled system. Here, the 'max' technique to de-fuzzification is used, which indicates that the control output will correspond to the fuzzy output value with the largest conceivable range of outcomes. This de-fuzzification method is selected based on the output's fuzzy membership functions.

$$\mu'_{V\ out}(v) = \max_{i-1}^{180} \left(\mu'_{Vi}(v)\right) \tag{4.4}$$

Figure 8 depicts the complete fuzzy logic controller. The diagram displays the four essential design and control units.

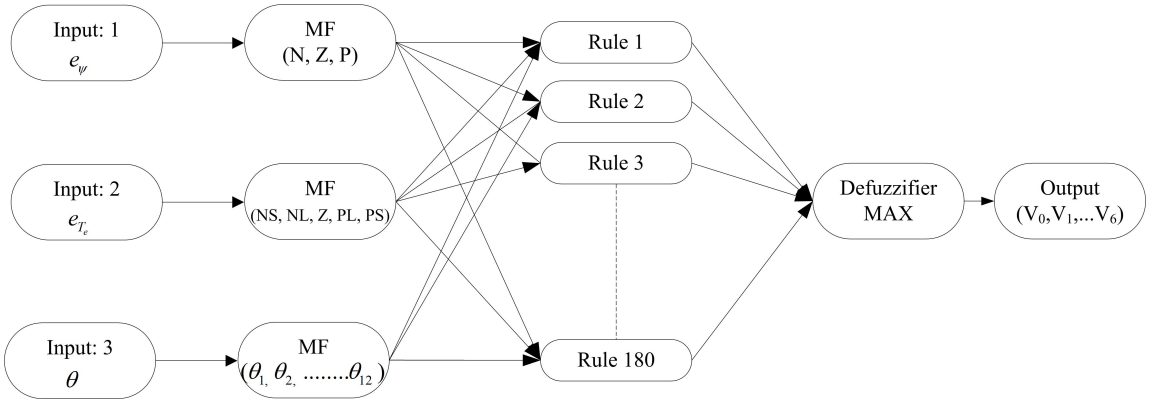

Figure 8. Complete fuzzy logic system.

5. Results and Discussion

A simulation test representing comparison between the traditional DTC and the proposed FDTC is presented here with considering various driving scenario. The simulations are carried out in Simulink/MATLAB environment. The simulations were conducted under the switching frequency f_s= 10 kHz with a simulation step size of 25 μs. The parameter of the induction motor used in the simulation study is listed in Table 5.

Table 5. Switching table for classical DTC.

Power:	50 Hp (37 kW)	$L_s = L'_r$:	0.724 (mH)
Voltage:	400 V	L_m:	27.11 (mH)
R_s:	82.33 $m\Omega$	Frequency (f):	50 Hz
R'_r:	50.3 $m\Omega$	Pole Pair (p):	2

A speed profile that is analogous to the one that can be found in applications involving electric vehicles is implemented for the purpose of control performance verification. To compare the performance simulation study of both the controllers is carried out.

From Figure 9, it is evident that the dynamics of both algorithms are similar; nevertheless, their ripples and harmonics distoration differs. For the identical operating conditions and reference stator flux, the FDTC torque ripple is 6.9% less than that of DTC. Even if the reference flux is identical for both, the flux ripple is reduced by 6.5%. Due to the exclusion of the hysteresis comparators, FDTC exhibits a 5.4% reduction in stator current THD compared to CDTC. With these results, it can be conclude that FDTC has a better operating performance with lower torque ripple, flux ripple, and THD.

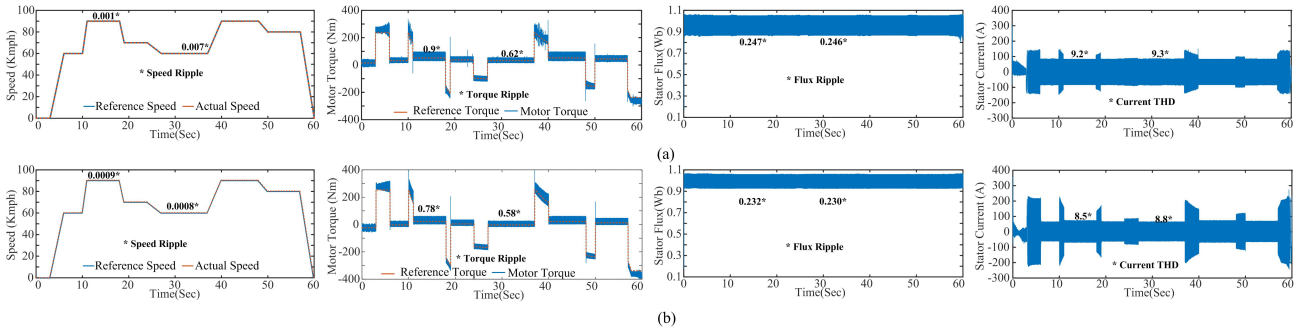

Figure 9. Performance of the vehicle with (a) DTC (b) FDTC.

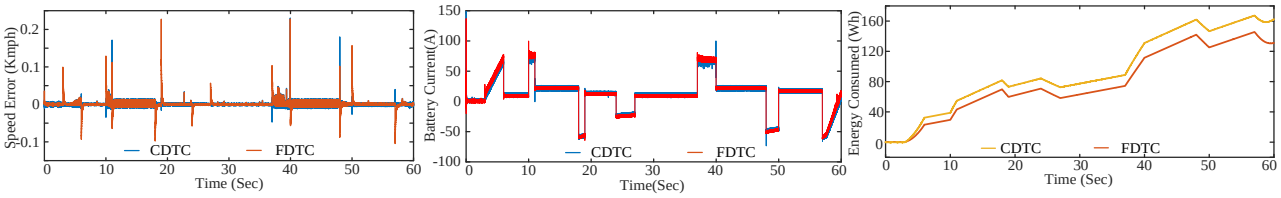

Figure 10. Comparison of CDTC and FDTC with (a) speed error (b) battery current (c) battery energy consumption.

Figure 10 compares the speed error, battery current, and battery energy consumption for DTC and FDTC. As demonstrated FDTC's speed error and battery current ripples are much lower than DTC's, resulting in a lower battery energy usage.

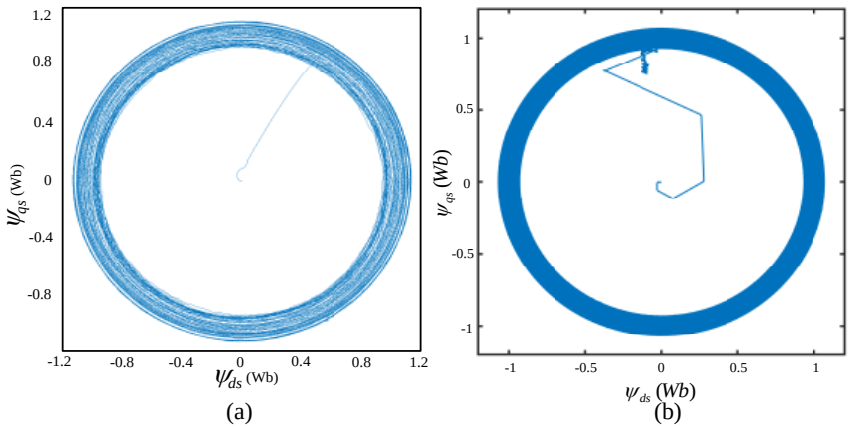

Figure 11. Circular trajectory of the stator flux (a) CDTC (b) FDTC

Figure 11 represents the circular trajectory of the stator flux for both classical DTC and proposed fuzzy DTC.

In order to further investigate the performance of the controller, a comprehensive examination of steady-state and transient operating situations is presented and compared to traditional DTC.

5.1. Performance during transient

To study the response of the controller during transient starting, braking, and speed reversal of the vehicle has been considered. A simulated comparison results of all the approaches are presented in Figure 12 and 13. Figure 12(a) depicts the torque and flux responses and the current ripples obtained during starting for both DTC and FDTC. As demonstrated, the vehicle was at standstill initially and starts to accelerate at t=2 seconds. There is a step change in torque produced during acceleration to meet the load demand. Even though the response time is identical, the data reveal a significant reduction in the ripple of torque, flux, and speed.

Figure 12(b) depicts the responses during braking for the traditional DTC and suggested FDTC. As demonstrated, the vehicle braked for a second to drop its speed from 60 kilometres per hour to 20 kilometres per hour. As the vehicle's speed decreases, the torque is reversed to ensure regenerative braking. Also, a reduction in ripple is seen, indicating that the proposed approach is superior to standard DTC.

Similarly, Figure 13 depicts the response of both the control systems during speed reversal. As mentioned, the motor generates negative torque enabling regenerative braking and faster vehicle reversal. As a result of regenerative braking, the battery consumes rather than delivers energy.

To numerically compare the performance of the controllers, the integral square error is computed for torque and speed for each of the three transient events and reported in Table 6. Results suggest a 10.34 %, 12.47 %, and 5.49 % improvement in the ISE of torque for starting, braking, and speed reversal, respectively. Similarly, these values for speed are 15.75 %, 17.1 %, and 9.39 %. These ripple reductions improve the error. Consequently, the ISE decreases. This demonstrates conclusively that the suggested approach has a superior dynamic response compared to traditional DTC.

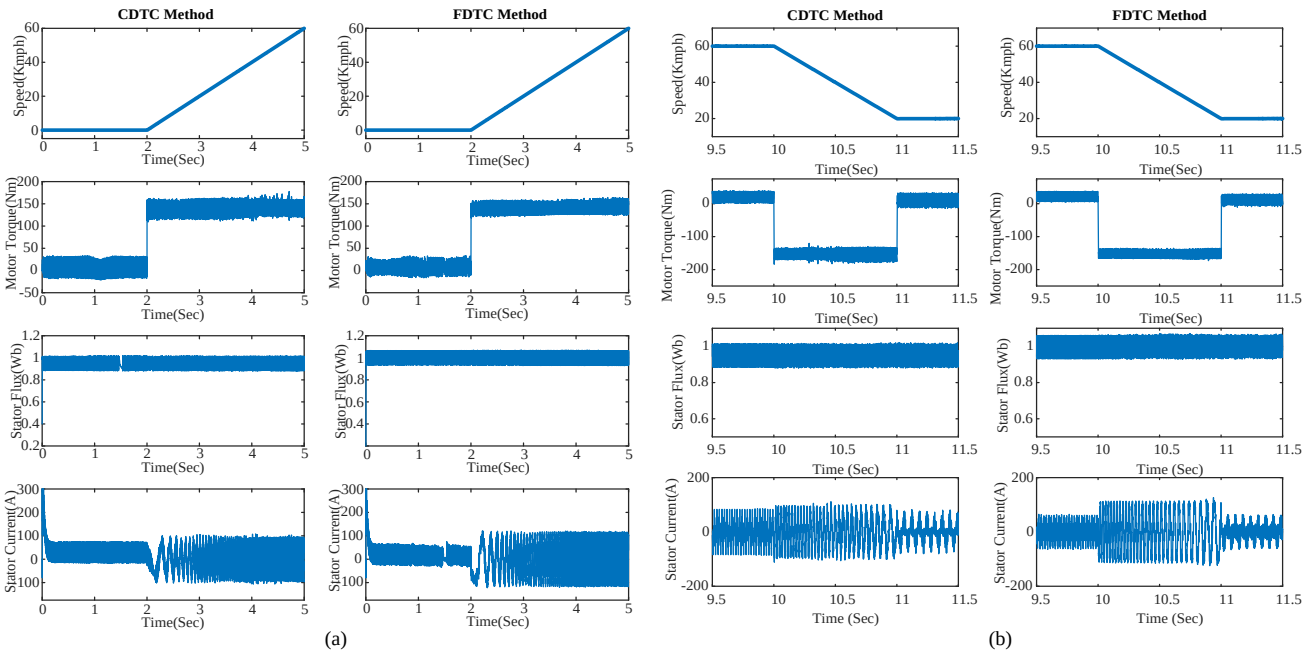

Figure 12. Performance comparison of CDTC and FDTC during (a) starting (b) braking.

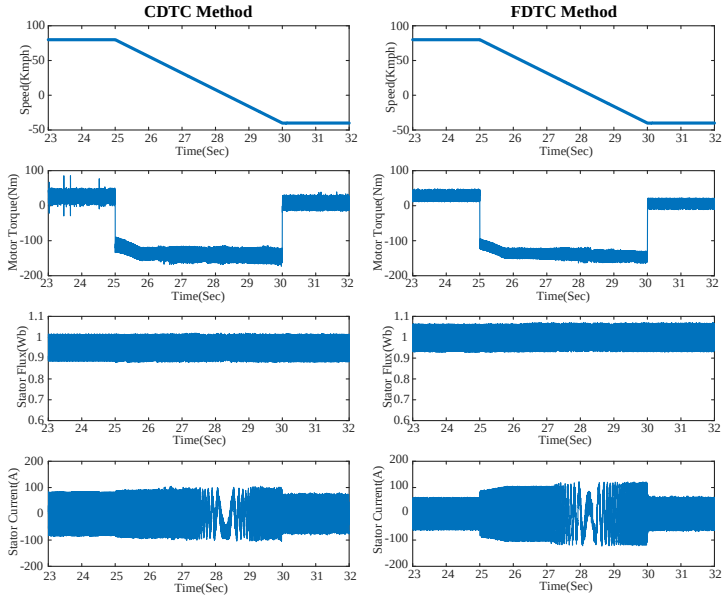

Figure 13. Performance comparison of CDTC and FDTC during speed reversal.

Table 6. ISE of torque and speed during transient condition.

Event	Parameter	CDTC	FDTC	Improvement (%)
Starting	Torque ($N.m^3$)	6.48e+07	5.81e+07	10.34
	Speed ($Kmph^3$)	23.5481	19.8395	15.75
Braking	Torque ($N.m^3$)	4.97e+07	4.35e+07	12.47
	Speed ($Kmph^3$)	5.2472	4.35	17.1
Speed Reversal	Torque ($N.m^3$)	9.48e+07	8.96e+07	5.49
	Speed ($Kmph^3$)	15.1584	13.7352	9.39

5.2. Steady-state performance

Here, we examine and compare the performance of the controller during steady-state response at low (20 kmph) and high (80 kmph) speeds. The steady-state performance of both control techniques is evaluated based on the torque, flux ripple, and current THD. Figure 14 (a) depicts the steady-state torque, flux, and current response for both at the low speed, and Figure 14 (b) depicts the responses at the high speed. Evidently, the proposed strategy reduces ripples and THD significantly at both speeds. The improvements are shown in Table 7, represents a 69 % reduction in torque ripple at high speed, and 19.09 % at low speed. Similarly, a 10.11 % reduction in flux ripple is found at high speed and a 2.36 % reduction at low speed. Due to the reduction in ripples there is a reduction of 17.58 % and 15.05 % of THD at high and low speed respectively.

To further examine the steady-state performance, Table 8 presents a comprehensive analysis conducted under various load and speed scenarios. The table demonstrates the increase in torque ripple, flux ripple, and THD that FDTC provides. The findings indicate that as speed and load increase, the improvements become more pronounced.

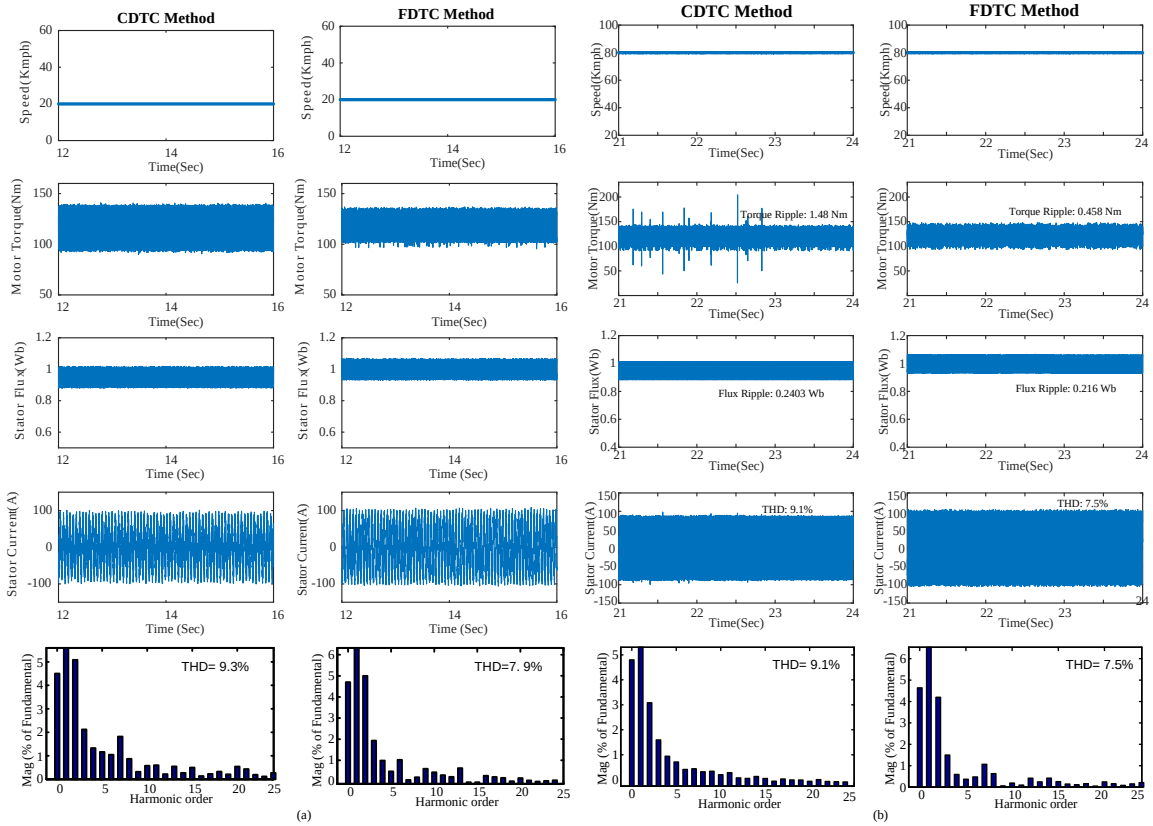

Figure 14. Performance comparison of CDTC and FDTC during (a)Low speed (b) High Speed.

Table 7. Performance evaluation during steady state.

Parameter	Characteristics	Speed	CDTC	FDTC	Improvement (%)
Torque	Ripple (N.m)	20 Kmph	0.44	0.356	19.09
		80 Kmph	1.48	0.458	69.05
Flux	Ripple (N.m)	20 Kmph	0.254	0.248	2.36
		80 Kmph	0.2403	0.216	10.11
Speed	Ripple (N.m)	20 Kmph	0.005	0.0004	92
		80 Kmph	0.006	0.0009	85
Current	%THD	20 Kmph	9.3	7.9	15.05
		80 Kmph	9.1	7.5	17.58

5.3. Performance with standard drive cycle

As depicted in Figures 15, the vehicle is simulated with EUDC and HWFET driving cycles to evaluate the performance of both controllers. The torque developed, stator flux and current, and energy consumed by the motor drive using both controllers are presented here. Due to the reduction in torque ripple and current distortion, the net energy consumption decreases by 8 percent for EUDC drive cycles and 9 percent for HWFET drive cycles as presented in Figure 15(a) and (b) respectively.

Table 8. Performance comparison of CDTC and FDTC with different load and speed condition.

Parameters		Torque Ripple(Nm)			Flux Ripple(Wb)			%THD		
Speed	**Load**	**CDTC**	**FDTC**	**% Change**	**CDTC**	**FDTC**	**% Change**	**CDTC**	**FDTC**	**% Change**
40 Kmph	No Load	3.5	2.9	17.14	0.25	0.241	3.6	10.2	9.3	8.82
	25%	0.886	0.567	36	0.25	0.24	4	9.6	8.9	7.29
	50%	0.482	0.314	34.85	0.249	0.24	3.61	9.1	7.8	14.29
	75%	0.35	0.216	38.29	0.2451	0.2345	4.32	8.6	8.1	5.81
	Full Load	0.276	0.2203	20.18	0.25	0.2358	5.68	8	7.5	6.25
60 Kmph	No Load	2.45	1.755	28.37	0.245	0.23	6.12	10.1	8.95	11.39
	25%	0.668	0.63	5.69	0.2467	0.2298	6.85	9.3	8.9	4.3
	50%	0.868	0.3438	60.39	0.2483	0.2297	7.49	9.3	7.6	18.28
	75%	0.58	0.29	50	0.25	0.2327	6.92	8.3	8.2	1.2
	Full Load	0.557	0.275	50.63	0.2494	0.2272	8.9	7.8	7.4	5.13
80 Kmph	No Load	2.79	1.88	32.62	0.2402	0.2174	9.49	10.1	8.8	12.87
	25%	0.809	0.717	11.37	0.247	0.2239	9.35	9.2	8.6	6.52
	50%	1.3	0.4598	64.63	0.241	0.2167	10.08	9.1	7.5	17.58
	75%	0.84	0.388	53.81	0.2481	0.2189	11.77	8.3	8.1	2.41
	Full Load	0.84	0.358	57.38	0.248	0.2197	11.41	7.7	6.8	11.69
100 Kmph	No Load	2.232	1.9328	13.41	0.2365	0.2105	10.99	10	8.6	14
	25%	1.3	0.988	24	0.2465	0.2168	12.05	9.1	8.2	9.89
	50%	0.814	0.621	23.71	0.245	0.2117	13.59	8.9	7.1	20.22
	75%	0.488	0.2614	46.43	0.247	0.2151	12.91	8	7.8	2.5
	Full Load	0.426	0.205	51.88	0.244	0.2139	12.34	8	7.1	11.25

6. Conclusions

In this paper, a novel fuzzy logic-based DTC strategy for a 50 hp induction motor-driven electric vehicle has been developed with the goal of reducing torque ripple and enhancing the DTC's dynamic performance. To increase the performance of the DTC, the suggested technique employed a 12-sector fuzzy controller instead of a hysteresis controller and a switching table. Using MATLAB/SIMULINK, a numerical comparison between the proposed DTC and the conventional DTC demonstrates a significant reduction in ripples. During low-speed, high-speed, and transient conditions, performance indices such as ripple torque, ripple flux, ripple speed, THD, and ISE were compared. The findings indicate:

- An improved steady state and dynamic stability.
- During low and high speed operation, a reduction of 19 % and 69 % in torque ripple and 2 % and 10 % in flux ripple was observed, which minimizes heating, vibration, and acoustic noise.
- The reduction in ripple improved the THD by 15 % in stator current which in result reduces the energy requirement by the vehicle.
- Reduction of ISE around 15 % during starting, braking, and speed reversal indicate improvement in dynamic performance.
- Improved performance indices when tested with standard drive cycles.

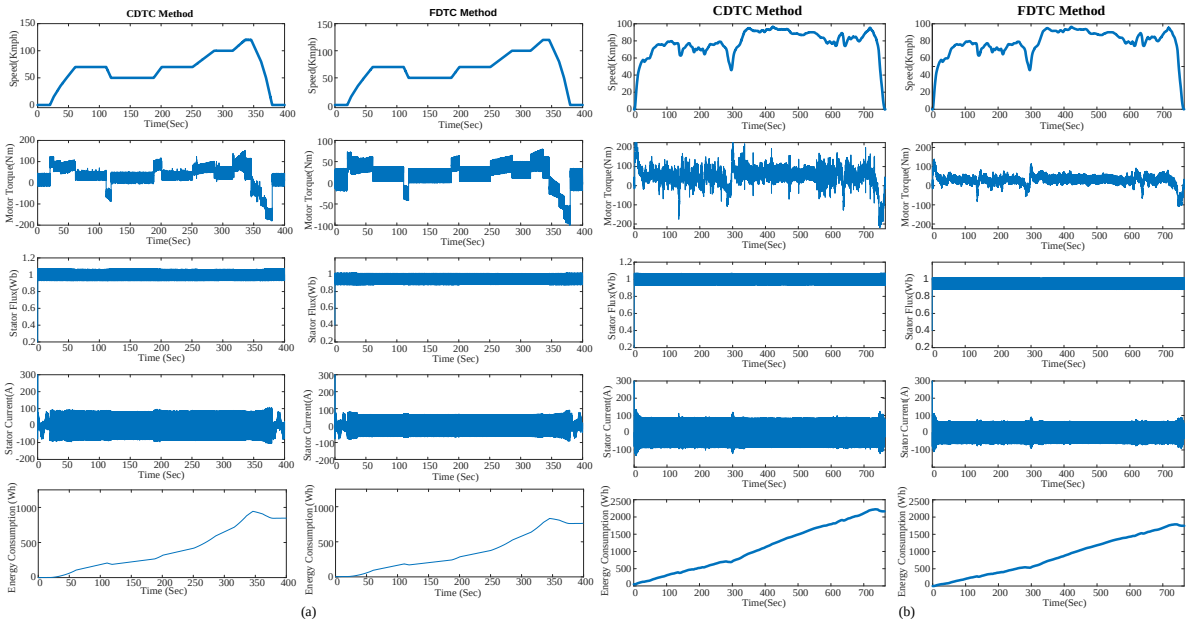

Figure 15. Performance comparison of CDTC and FDTC during (a)EUDC drive cycle (b) HWFET drive cycle.

The proposed approach also has some limitations and scope of further improvements as follows:

- There are no specific rules for selecting the number of MFs and fuzzy rules, it is completely based on trial and error approach.
- The performance of the DTC can be improved by selecting appropriate number and type of MFs.
- The computational time and system complexity is higher compare to DTC.
- It required further improvement in the controller to increase the accuracy.
- Various state of the art optimization algorithms may be used for the speed controller and to select the optimal switching vector to further improve the performance.
- The fixed stator flux employed may not be adequate for the efficient regulation of a wide speed and torque range.
- An optimization algorithm for selection of optimal stator flux corresponds to the driving scenario may be used.
- The voltage vector selection is based on torque and flux error and position of the stator flux angle, which can introduce variable switching frequency.
- Additional AI-type controllers may be used for comparison with FDTC in EV applications.
- The proposed method with EV application can be validated experimentally with an FPGA, DSP, or dspace platform.
- In simulation studies, high performance computers with parallel computing are used for AI-based approaches to improve the dynamic response, whereas in practise, for a dynamically changing driving scenario with limited computing capability, the computational time became a burden, leading to the introduction of lookup tables to improve the response time in many applications.

Abbreviation

AI	Artificial Intelligence
CDTC	Classical Direct Torque Control
DOM	Degree of Membership
DTC	Direct Torque Control
EUDC	Extra Urban Driving Cycle
EV	Electric Vehicles
FDTC	Fuzzy Direct Torque Control
FIS	Fuzzy Interface System
ANN	Artificial Neural Network
GA	Genetic Algorithm
SMO	Sliding Mode Observer
Kmph	Kilometer per hour
FLC	Fuzzy Logic Controller
HWFET	EPA Highway Fuel Economy Test Cycle
IFOC	Indirect Field-Oriented Control
IM	Induction Motor
ITAE	Integral time-weighted absolute error
SVM	Space Vector Modulation
THD	Total Harmonic Distortion
VSI	Voltage source inverter
ISE	Integral Square Error
PI	Proportional Integral
SMC	Sliding Mode Controller

Nomenclature

P_v	Net force on vehicle
F_{te}	Taction force
F_{ro}	Rolling resistance force
F_{cr}	Hill-climbing force
F_{la}	Acceleration force
F_{ad}	Aerodynamic drag force
a	Acceleration of the vechile
v	velocity of the vehicle
m	Mass of the vehicle
ω_m	Angular mechanical speed of vehicle
w_{wheel}	Wheel speed
T_{wheel}	Wheel torque
ψ_s	Stator Flux
ψ_r	Rotor Flux
R_s	Stator resistance
L_s	Stator self indictance
L_r	Rotor self indictance
L_m	Mutual Inductance
T_e	Electromagnetic torque
σ	Leakage factor
V_s	Stator voltage
ΔT_e	Torque error
$\Delta\psi_s$	Flux error
A_i, B_i, C_i	Fuzzy sets

Conflict of interest

The authors declares no conflict of interest.

References

1. De Klerk ML & Saha AK (2021) A comprehensive review of advanced traction motor control techniques suitable for electric vehicle applications. *IEEE Access*. https://doi.org/10.1109/ACCESS.2021.3110736
2. Karki A, Phuyal S, Tuladhar D, et al. (2020) Status of pure electric vehicle power train technology and future prospects. *Applied System Innovation* 3: 35. https://doi.org/10.3390/asi3030035

3. Chapman L (2007) Transport and climate change: a review. *J Transp Geogr* 15: 354–367. https://doi.org/10.1016/j.jtrangeo.2006.11.008
4. Sanguesa JA, Torres-Sanz V, Garrido P, et al. (2021) A review on electric vehicles: Technologies and challenges. *Smart Cities* 4: 372–404. https://doi.org/10.3390/smartcities4010022
5. Chau KT (2015) *Electric vehicle machines and drives: design, analysis and application*, John Wiley & Sons. https://doi.org/10.1002/9781118752555
6. Nisha GK & Lakaparampil ZV (2022) Induction Machine Characteristics Control in Field Weakening Region for Propulsion Application. *Power Electronics and High Voltage in Smart Grid*, 283–297. Springer, Singapore. https://doi.org/10.1007/978-981-16-7393-1_23
7. Alsofyani IM, Idris NRN & Lee KB (2017) Dynamic hysteresis torque band for improving the performance of lookup-table-based DTC of induction machines. *IEEE T Power Electr* 33: 7959–7970. https://doi.org/10.1109/TPEL.2017.2773129
8. El Ouanjli N, Derouich A, El Ghzizal A, et al. (2019) Modern improvement techniques of direct torque control for induction motor drives-a review. *Prot Contr Mod Pow* 4: 1–12. https://doi.org/10.1186/s41601-019-0125-5
9. El Ouanjli N, Mahfoud S, Derouich A, et al. (2022) Speed Sensorless Fuzzy Direct Torque Control of Induction Motor Based MRAS Method. In *International Conference on Digital Technologies and Applications*, 779–790. Springer, Cham. https://doi.org/10.1007/978-3-031-02447-4_80
10. Ghamri A, Boumaaraf R, Benchouia MT, et al. (2020) Comparative study of ANN DTC and conventional DTC controlled PMSM motor. *Math Comput Simulat* 167: 219–230. https://doi.org/10.1016/j.matcom.2019.09.006
11. Ghezouani A, Gasbaoui B & Ghouili J (2018) Modeling and sliding mode DTC of an EV with four in-wheel induction motors drive. In *2018 International Conference on Electrical Sciences and Technologies in Maghreb (CISTEM)*, 1–9. IEEE. https://doi.org/10.1109/CISTEM.2018.8613379
12. El Daoudi S, Lazrak L, Benzazah C, et al. (2019) An improved Sensorless DTC technique for two/three-level inverter fed asynchronous motor. *International Review on Modelling and Simulations (IREMOS)* 12: 322–334. https://doi.org/10.15866/iremos.v12i5.17394
13. Tarbosh QA, Aydoğdu Ö, Farah N, et al. (2020) Review and investigation of simplified rules fuzzy logic speed controller of high performance induction motor drives. *IEEE Access* 8: 49377–49394. https://doi.org/10.1109/ACCESS.2020.2977115
14. El Ouanjli N, Motahhir S, Derouich A, et al. (2019) Improved DTC strategy of doubly fed induction motor using fuzzy logic controller. *Energy Rep* 5: 271–279. https://doi.org/10.1016/j.egyr.2019.02.001
15. El Daoudi S, Lazrak L, El Ouanjli N, et al. (2021) Sensorless fuzzy direct torque control of induction motor with sliding mode speed controller. *Comput Electr Eng* 96: 107490. https://doi.org/10.1016/j.compeleceng.2021.107490
16. Sudheer H, Kodad SF & Sarvesh B (2018) Improvements in direct torque control of induction motor for wide range of speed operation using fuzzy logic. *Journal of Electrical Systems and Information Technology* 5: 813–828. https://doi.org/10.1016/j.jesit.2016.12.015

17. El Daoudi S & Lazrak L (2021) Comparison between PI-DTC-SPWM and fuzzy logic for a sensorless asynchronous motor drive. *Prot Contr Mod Pow* 6: 1–13. https://doi.org/10.1186/s41601-021-00216-9
18. El Ouanjli N, Motahhir S, Derouich A, et al. (2019) Improved DTC strategy of doubly fed induction motor using fuzzy logic controller. *Energy Rep* 5: 271–279. https://doi.org/10.1016/j.egyr.2019.02.001
19. Tidke R & Chowdhury A (2022) Quasi ZSI-Fed Sliding Mode Control-based Indirect Field-Oriented Control of IM Using PI-Fuzzy Logic Speed Controller. *Electrica* 22: 70–85. https://doi.org/10.5152/electrica.2021.21081
20. Gdaim S, Mtibaa A & Mimouni MF (2014) Design and experimental implementation of DTC of an induction machine based on fuzzy logic control on FPGA. *IEEE T Fuzzy Syst* 23: 644–655. https://doi.org/10.1109/TFUZZ.2014.2321612
21. Ammar A (2019) Performance improvement of direct torque control for induction motor drive via fuzzy logic-feedback linearization: Simulation and experimental assessment. *COMPEL-The international journal for computation and mathematics in electrical and electronic engineering*. https://doi.org/10.1108/COMPEL-04-2018-0183
22. Adegbohun F, Von Jouanne A, Phillips B, et al. (2021) High performance electric vehicle powertrain modeling, simulation and validation. *Energies* 14: 1493. https://doi.org/10.3390/en14051493
23. Reddy KS & Veeranna SB (2020) Design Parameters of Electric Vehicle. In *2020 International Conference on Power Electronics & IoT Applications in Renewable Energy and its Control (PARC)*, 14–21. IEEE. https://doi.org/10.1109/PARC49193.2020.236548
24. Takahashi I & Noguchi T (1986) A new quick-response and high-efficiency control strategy of an induction motor. *IEEE T Ind Appl* 5: 820–827. https://doi.org/10.1109/TIA.1986.4504799
25. Depenbrock M (1987) Direct self-control (DSC) of inverter fed induktion machine. In *1987 IEEE Power Electronics Specialists Conference,* 632–641. IEEE. https://doi.org/10.1109/PESC.1987.7077236

AIMS Press